THEORETICAL AND EXPERIMENTAL INVESTIGATION OF AERATION PHENOMENON IN THE AIR-WATER INTERFACE

Adele Vaideliene, Daiva Rimkuviene

Aleksandras Stulginskis University, Studentu str. 10, Kaunas r., LT-53361, Lithuania

Abstract

This paper deals with physics of water aeration. Because water aeration highly influences the process of polluted water treatment as well as the process of water self-purification it becomes an important factor determining the amount of air entrained in the water. Falling water flow produces air bubbles and water droplets mixture in the air-water interface. This mixture develops in the course of time. A new method for determination of the amount of air entrained in the water was presented. The method was based on digital image processing. The method allows determination of the dynamics of air entrainment depending on several parameters of the nozzle as well as on the height of falling water flow.

Key words: *water, aeration, bubbles, droplets, mixing, diffusion, layers*

1. INTRODUCTION

Many physical processes occur due to the air and water interaction in water reservoirs. Among them, the depth of air entrapment is a very important element in the aeration process.

Pollution of open reservoirs water also is the result of technologies, which are developing with extremely high rate. Thus, anthropogenic activity highly influences common environmental processes [1-4]. With production intensity increasing, influence of human activity on environment also increases. Atmospheric pollution with toxic substances generates acid rains, destroys the ozone layer and creates more undesirable phenomena. Biogenic and toxic substances from sewer towns, industrial plants and intensive agriculture areas infiltrate into natural water reservoirs. Encompassing theoretical and experimental investigations of each contributing parameters will lead to significant solutions. The main goal of water cleaning is to eliminate the results of above mentioned influences. Quantitative evaluation of atmosphere and natural water pollution, i.e. determination of pollution degree, amount and derivation of sediments can be successfully completed only after thorough investigation of combined processes of air and water mass transfer, diffusion, heat transfer, gas and fluid flow [5-10]. These processes can be described by common equations of motion, continuity, heat and impurities balance. These equations usually are applied for description of gas and fluid flows. The most part of these phenomena were investigated and results of the investigations were successfully used practically. To less investigated or at all not investigated processes should be assigned processes that occur in the open reservoirs air-water interface. These processes are extremely important due to their influence on water aeration, which on its own turn determinates rate and amount of water self-purification process [11-14]. Full understanding of water aeration mechanism also allows improvement of water cleaning methods and control of water pollution treating [15-17].

Processes occurring in the air-water interface first of all depend on conditions under which one or another process occurs. Interaction between surfaces of air and water also depends on the fluid flow nature, which can be laminar or turbulent. Turbulent flow stimulates air bubbles generation and creates conditions for their entrainment in water [18-22]. Investigations of water flows interaction with air were undertaken short time. The first successful experiments of air bubbles entrainment in water were performed only in the middle of the twentieth-century. Then air bubbles entrainment in water was considered as diffusion air bubbles in water, though now is known that there are many more processes. Water flowing trough wears and forcing trough hydropower's turbines [23-25] mix with air and create mixtures which consist of air bubbles and water droplets. Resulting mixture air bubbles and water droplets is commonly called "white water" due to its visual effect. For experimental investigation air bubbles and water droplets mixture can be produced with vertically falling water jets.

2. RESEARCH METHODOLOGY

2.1. Inception of air entrapment

Water flow falling on to the free water surface deforms its surface and, sequentially, creates turbulent flows, which push the air into deeper water layers (fig. 1).

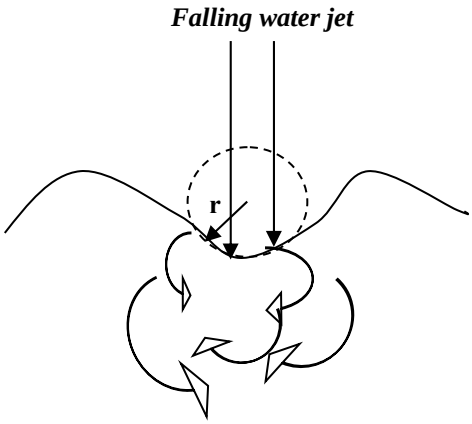


Fig. 1. Deformation of water surface with the falling vertical jet

Entrapment of air bubbles happens only when the turbulent shear stress is sufficiently high to overcome surface tension and buoyancy effect. Due to disturbed free surface, small turbulent structures with major eddies appear in the lower water layers. If the turbulent energy is sufficiently high to break through the free water, air bubbles can be entrapped. Naturally, for breaking through the free surface, the turbulent shear stress must be higher than the resisting surface tension force per square unit. Mathematically it can be expressed as follows [26]:

$$\left|\rho_v \cdot v_i \cdot v_j\right| > \sigma \frac{\pi \cdot (r_1 + r_2)}{A} \tag{1}$$

where ρ_v – water density, v – turbulent velocity fluctuation, (i, j) is the directional tensor, σ – water surface tension, $\pi(r_1+r_2)$ – perimeter along surface tension, r_1 and r_2 are the two radii of the free surface deformation, A – surface area.

2.2. Experimental Setup

The companion experiment was performed under laboratory conditions with the vertical jet hitting free water surface in a transparent cylindrical vessel. The setup of experiment is shown in the figure 2.

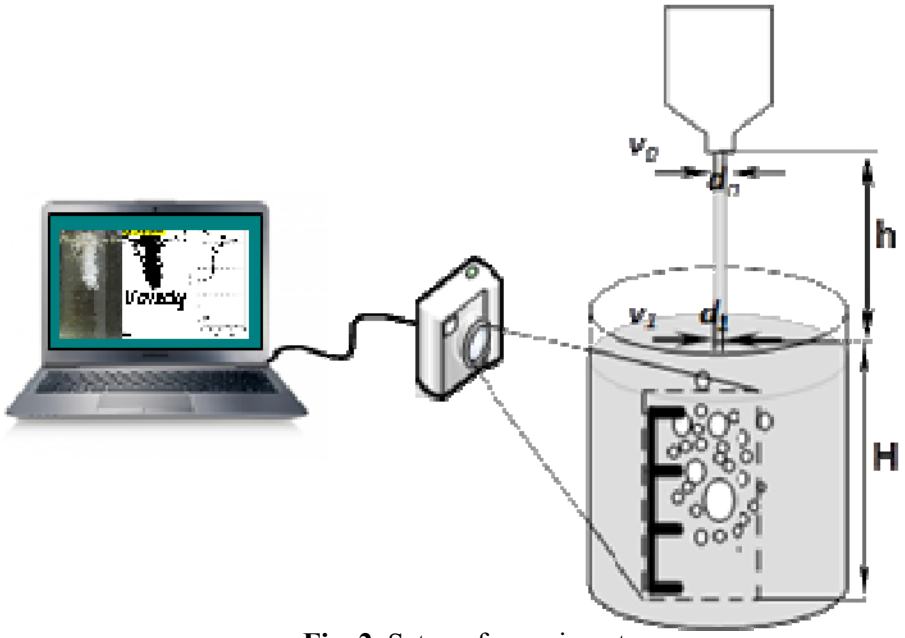


Fig. 2. Setup of experiment

Dimensions of the cylinder were: diameter – 18 cm and depth – 18.5 – cm. Experimentation utilized digital processing of images registered by the Canon PowerShot SX20IS camera connected to computer. Diameter of the jet nozzle was d_0, initial velocity of jet $v_0=0$, v_1 – velocity of the jet at the moment of its contact with the water surface, h – the height of the falling jet i.e. distance from the nozzle tip to the water surface. h was varied in steps of 0.25 m from $h = 0.25$ m to $h = 1$ m, H – air penetration depth (m). Also the jet nozzle diameter d_0 was varied from 0.003 m ÷ 0.008 m. Additional information is given in the table 1.

In all experiments the same volume of water V was poured into test cylinder. The average amount of water Q_w (m^3/s) flowing through the jet nozzle can be calculated as $Q_w=V/t$, where t – elapsed time to complete water pouring. Also Q_w can be calculated as:

$$\begin{cases} Q_w = v_0 \cdot \pi \cdot \left(\frac{d_0}{2}\right)^2 \\ Q_w = v_1 \cdot \pi \cdot \left(\frac{d_1}{2}\right)^2 \end{cases} \quad (2)$$

Equations (2) give:

$$\frac{v_1}{v_0} = \frac{d_0^2}{d_1^2} \quad (3)$$

From the energy conservation law it follows:

$$v_1^2 = v_0^2 + 2g \cdot h \tag{4}$$

were g – free fall acceleration, m – mass of poured water, d_0 and d_1 are shown in Fig. 2.

As can be seen from Fig. 2, camera takes pictures of air bubbles and water droplets mixture created by a vertical jet. Computer analyzes received optical images and determines air bubbles concentrations. For digital image processing Library Python 2.7 program was used.

Table 1. Initial data of experiment

d_0=0.003 m; Q_w=1.5543·10^{-5} m^3/s				d_0=0.004 m; Q_w=2.2382·10^{-5} m^3/s			
h, m	v_1, m/s	d_1, m	Fr_1	h, m	v_1, m/s	d_1, m	Fr_1
0.25	2.2	0.0026	13.8	0.25	2.2	0.0036	11.7
0.5	3.1	0.0023	20.6	0.5	3.1	0.003	18.1
0.75	3.8	0.0101	26.7	0.75	3.8	0.0027	23.4
1.0	4.4	0.0097	31.6	1.0	4.4	0.0025	28.1

d_0=0.007 m; Q_w=7.9856·10^{-5} m^3/s				d_0=0.008 m; Q_w=1.0778207·10^{-4} ^{3}/s			
h, m	v_1, m/s	d_1, m	Fr_1	h, m	v_1, m/s	d_1, m	Fr_1
0.25	2.2	0.0068	8.5	0.25	2.2	0.0079	7.9
0.5	3.1	0.0057	13.1	0.5	3.1	0.0067	12.1
0.75	3.8	0.0052	16.8	0.75	3.8	0.006	15.7
1.0	4.4	0.0048	20.3	1.0	4.4	0.006	18.1

Experimental methodology is depicted in Fig. 3. At the left side the real image of the air bubbles and water droplets mixture is shown. At the right side the modified image with the air bubbles changed to the black spots is presented. Visual analysis of the left image shows that the air bubbles are much brighter than the background. This feature allows evaluation of the air bubble concentration in the water.

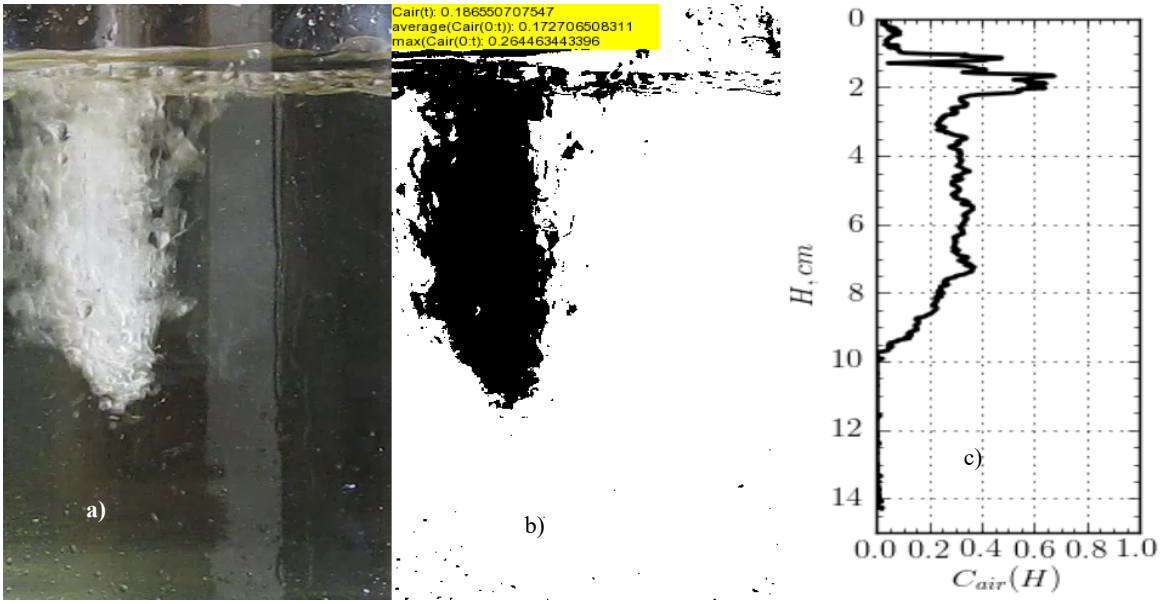


Fig. 3. Change of air entrainment

As can be seen from Fig. 3 the image representing the experiment consists of three parts. On the left side (Fig 3a) is a real image of air bubbles and water droplets mixture. The central part of figure (Fig 3b) represents modified image of air entrainment in the water. Computer program Python 2.7 code optical analyzes received images and presents data. The black digital image is the modified image of air bubbles and the white image is of water droplets [27]. On the right side of the figure (Fig 3c) the change of concentration of air entrained in depth and width is represented.

3. RESULTS AND DISCUSSIONS

Vertical water flow (jet) hitting the free water surface causes mixing of water and air. As a result of this mixing air is entrained in the deeper water layers. Air-water mixture exists not only under the air-water interface but also above this interface when under the water surface the air-water mixture bloats, air bubbles rises up and is removed from water. Falling water also can generate water sprays that can evaporate or fall back to the water surface. Fallen sprays can knock out new water sprays or be absorbed by the water. These processes were included in the here in developed a mathematical model by A.Vaideliene and A. Galdikas [28]. The model has significant relevance to development and improvement of aeration process and can be used for practical purposes.

All of the discussed and described processes [28] due to the air-water interaction can be summarized by an overall mathematical model, equation (5). This model includes the processes of air entrapping, air elimination, water sputtering and resorption:

$$\begin{cases} \dfrac{d\varphi_2^{(k)}}{dt} = \left(\dfrac{d\varphi_2^{(k)}}{dt}\right)_{entrain} + \left(\dfrac{d\varphi_2^{(k)}}{dt}\right)_{elimin} + \left(\dfrac{d\varphi_2^{(k)}}{dt}\right)_{sput\text{-}evapor} + \left(\dfrac{d\varphi_2^{(k)}}{dt}\right)_{resorb} \\ \dfrac{d\varphi_1^{(k)}}{dt} = \left(\dfrac{d\varphi_1^{(k)}}{dt}\right)_{entrain} + \left(\dfrac{d\varphi_1^{(k)}}{dt}\right)_{elimin} + \left(\dfrac{d\varphi_1^{(k)}}{dt}\right)_{sput\text{-}evapor} + \left(\dfrac{d\varphi_1^{(k)}}{dt}\right)_{resorb} \end{cases}, k = K, K-1, \ldots, m, \ldots, 2, 1 \quad (5)$$

The entire air entrainment zone is represented by the *K* layers which can be filled with air, water or sum of them. Normalized filling function of *j*-th layer was introduced:

$$\varphi^{(j)}=\varphi_1^{(j)}+\varphi_2^{(j)}=1,\ when\quad j=1,2,...,K-1,K,K+1 \tag{6}$$

where $\varphi_1^{(j)}$ and $\varphi_2^{(j)}$ are functions of a layer filling with water and air, respectively. Rate of change of these functions $\varphi_1^{(j)}$ $\varphi_2^{(j)}$ can be described as a sum of equations of entrainment, removal, sputtering, evaporation and resorption rate.

Solutions of equations (5) can be used for determining concentrations of air bubbles and water droplets due to turbulent flows created by a free vertical water jet hitting the free water surface. This model was verified by using data from the below-described experiment.

3.1. Comparison of experimental and theoretical results

The amount of entrapped air (Fig. 2) depends on diameter of nozzle d_0, the height of falling jet *h*, diameter d_1, and velocity v_1. Small sputtering at the surface of water also influences the amount and distribution of entrapped air. Influences of all these factors can be determined theoretically by using equations (5) or experimentally. We used both ways and compared the obtained results. For comparing the theoretical and experimental results we used our experimental data as well as the data presented by others researchers [29-31].

As a boundary condition we took the monolayer *k=m=60*. In this study we define, that the last layer filled with air and water is the *m*-th layer while the *(m+1)*-th monolayer is filled only with water. Using equations from (4.13) we took the initial and boundary conditions corresponding to *t = 0*: $\varphi_2^{(k)}(0)=1,\ \varphi_1^{(k)}(0)=0$ when $1\le k<m$ and $\varphi_2^{(k)}(0)=0,\ \varphi_1^{(k)}(0)=1$, $\varphi_1^{(m)}(t)=\varphi_1^{(m+1)}(t)$, when $m\le k\le K$.

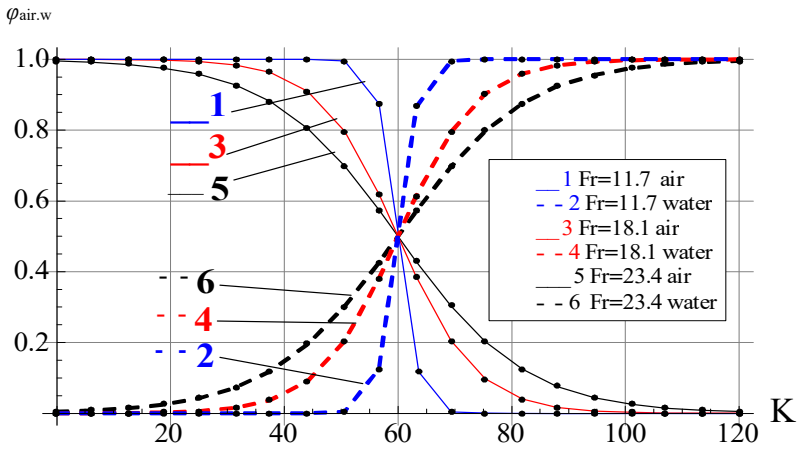


Fig. 4. Air and water distribution in layers for different Froude numbers. Modeling was done according to equations (5)

Figure 4 shows that with an increasing monolayer numbers, concentration of air decreases from one to zero and is dependent on the Froude number. Also, can be seen that the 60-th layer is the air-water interface layer. Because the water concentration variation is a reciprocal process, water concentration changes from zero to one.

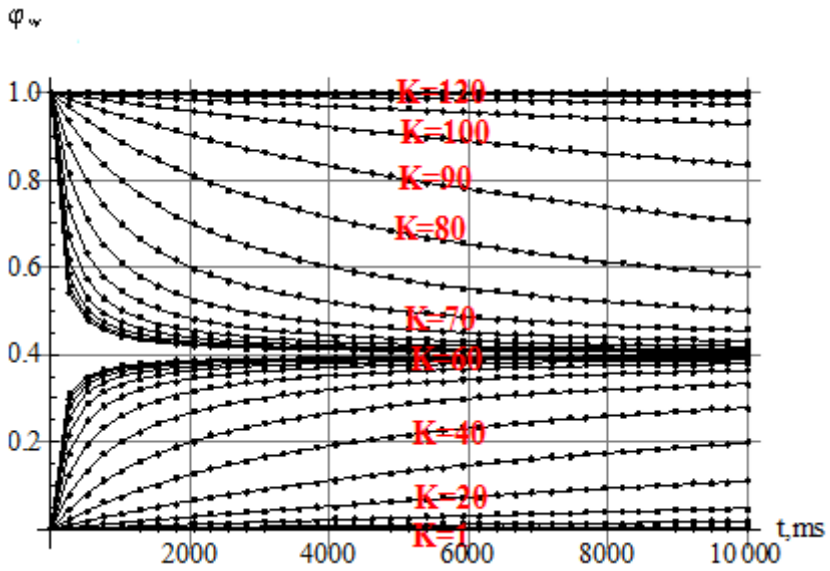


Fig. 5. Dependencies of individual layers (*K*) filling with water for *Fr*=5 were established by solving equation (5)

Figures 5 and 6 show air and water distribution dependences on time in separate layer. The boundary layer between air and water is at *K*=60. Just at the beginning of air entrapment its concentration in separate monolayer decreases from 1.0 (starting from *K* th monolayer) to 0.0 due to formation of the mixture of air bubbles and water droplets. Close to the *K*=60 layer new adjacent layers are filled with air bubbles and water droplets mixture from above and below the interface.

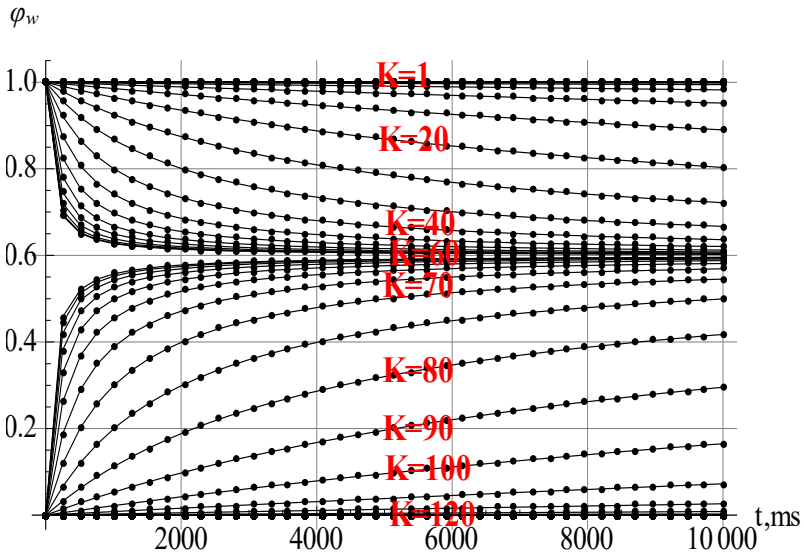


Fig. 6. Dependencies of individual layers (*K*) filling with air for *Fr*=5 were established by solving equation (5)

With decreasing amount of water, the amount of air increases in adjacent layers. As it can be seen from figure 5 the first layer being filled with water at time t is nearly 0.0, when filling with air of time t (Fig. 6) approaches 1.0.

In figure 7 shows the air and water concentrations distribution at various in depths by employing equation (5). In solving this equation φ_{air}, φ_w (air and water concentrations) in layers are distributed according to Gaussian function and Fr=9.2.

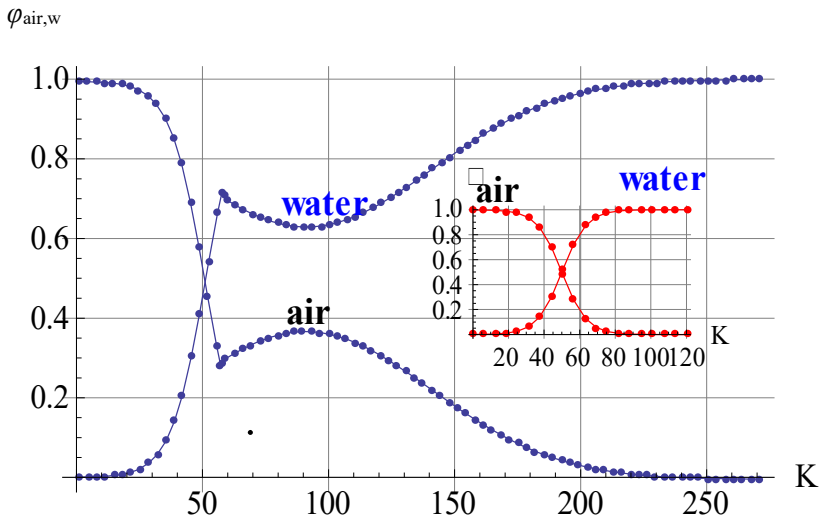


Fig. 7. Air and water concentrations distribution in depth

It can be seen from Fig. 7 the curve on the bottom (blue) shows concentration of entrapped air while the upper curve shows changes in water concentration. The concentration of air entrapped in water initially increases and then after reaching maximum starts to decrease to zero. Initially, the water concentration φ decreases and after reaching minima starts to increase to 1.0. Curves (red) of inserted diagram show entrapped air and water concentration's variation in monolayer.

To validate the developed model equation (5) was employed with the same initial conditions used in experimentation. Theoretical values correlate very well with the experimental data shown in Figure 8.

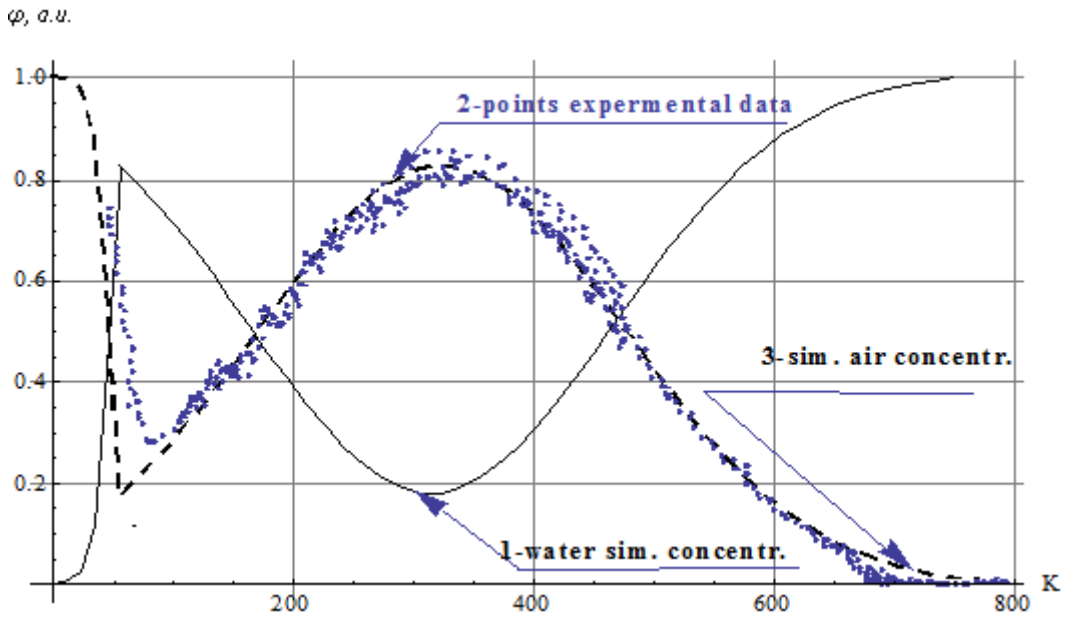


Fig. 8. Air and water concentration dependences on layer numbers. Continuous curve 1 – water concentration variation, dotted curve 3 – air concentration variation calculated according equation (5). Dashed curve 2 – experimental data with d_0=0.003 m; d_1=0.0026 m; v_1=4.4 m/s; h=1.0 m; Fr=18.1

Figure 8, shows concentration of air bubbles based on equation (5). The maxima is reached when K=300 and Fr=18.1. Verifying this case by experiment with the initial data set of d_0=0.003 m; d_1=0.0026 m; v_1=4.4 m/s; h=1.0 m; Fr=18.1 the maximum concentration was 0.85431. The calculated maximum according to equation (5) was 0.825. Air concentration maximum (Fig. 8 – dotted line) corresponds to the water concentration minimum (Fig. 8 – continuous line). Comparison of theoretical and experimental dependences of air and water concentrations shows an excellent correlation.

4. CONCLUSIONS

1. Air entrainment in water plays important role in processes of water treatment and water self-purification.
2. Initial conditions of air bubbles and water droplets mixing determine dynamics of this process that on its own turn determine amount of air bubbles entrained in water.
3. Dynamics of air bubbles and water droplets mixing can be visualized and analyzed by means of digital images processing.
4. Analyse of images taken at many different moments of mixture developing allows determine amount of air entrained dependences on many parameters, and first of all on height of water flow fall and on nozzle parameters.

REFERENCES

1. Jeffery, C. D.; Woolf, D. K.; Robinson, I. S.; Donlon, C. J. 1-D modelling of convective CO_2 exchange in the Tropical Atlantic. Ocean Modelling 19, 2007, p. 161–182.
2. Jeffery, C. D.; Robinson, I. S.; Woolf, D. K. Tuning a physically-based model of the air–sea gas transfer velocity. Ocean Modelling 31, 2010, p. 28–35.

3. Moioli, S.; Pellegrini, L. A. Regeneration Section of CO_2 Capture Plant by MEA Scrubbing with a Rate-Based Model. Chemical Engineering Transactions 32, 2013, p. 1849-1854.
4. Chiba, D.; Baschek, B. Effects of Langmuir cells on bubble dissolution and air-sea gas exchange. J. Geopphys. Res. 115, 2010, C10046.
5. Wanninkhof, R.; Asher, W. E.; Ho, D. T.; Sweeney, C.; McGillis, W. R. Advances in quantifying air-sea gas exchange and environmental forcing. Annu. Rev. Mar. Sci., 1, 2009, p. 213-244.
6. Rowe, M. D.; Perlinger, J. A. Micrometeorological measurement of hexachlorobenzene and polychlorinated biphenyl compound air-water gas exchange in Lake Superior and comparison to model predictions. Atmospheric Chemistry and Physics Discussions 12, 2012, p. 983–1017. DOI:10.5194/acpd-12-983-2012
7. Johnson, M. T. A numerical scheme to calculate temperature and salinity dependent air-water transfer velocities for any gas. Atmospheric Chemistry and Physics Discussions 7, 2010, p. 251–290.
8. Cole, J. J.; Bade, D. L.; Bastviken, D.; Pace, M. L.; Van de Bogert, M. Multiple approaches to estimating air-water gas exchange in small lakes. Limnol. Oceanogr.: Methods 8, 2010, 285–293.
9. Cole, J. J.; Bade, D. L.; Bastviken, D.; Pace, M. L.; Van de Bogert, M. Multiple approaches to estimating air-water gas exchange in small lakes. Limnol. Oceanogr.: Methods 8, 2010, p. 285–293.
10. Chatterjee, S. G. A Theoretical Analysis of Dissolved – Gas Transfer to the Bulk Liquid in Gas Absorption with a First – Order Reaction. Indian Institute of Chemical Engineers, 51 (3), 2009, p. 177-193.
11. Csanady, G. T. The role of breaking wavelets in air-sea gas transfer. J. Geophys. Res. 95, Article first published online: 2012, p. 749-759. DOI: 10.1029/JC095iC01p00749
12. Delbos, S.; Weitbrecht, V.; Bleninger, T.; Grand, P. P.; Chassaing, E.; Lincot, D.; Kerrec, O.; Jirka, G. H. Homogeneous turbulence at an electrodeposition surface induced by randomly firing jet arrays. Exp. Fluids 46, 2009, p. 1105–1114.
13. Back, D. D.; McCready, M. J. Effect of small-wavelength waves on gas transfer across the ocean surface. *J. Geophys. Res.* 93, Article first published online: 2012, p. 5143-5152. DOI: 10.1029/JC093iC05p05143
14. Emiroglu, M. E N. Estimating Flow Characteristics of Different Weir Types and Optimum Dimensions of Downstream Receiving Pool. Journal of Hydrology and Hydromechanics, 2010, p. 245–260.
15. Vaideliene, A. Hydropower plants influence on downstream river's water quality // Proceedings of the 10th International Congress on Mechanization and Energy in Agriculture, 14-17 October 2008, Antalya-Turkiye / Akdeniz University. faculty of Agriculture. Department of Agricultural. Antalya : Yeni Gun Press, 2008, p. 557-561.
16. Vaideliene, A.; Galdikas, A.; Vaidelys, V. Water turbulence after hydropower's plants influence on gas diffusion processes // Proceedings of The Union of Scientists - Rousse : Energy Efficiency and Agricultural Engineering : conference prpceedings, Rousse, Bulgaria, 1-3 October, 2009. Rousse : University of Rousse. 2009, p. 883-889.
17. Vaideliene, A.; Vaidelys, V. Investigation of pysical processes taking place on the open channel's air-water interface // Research People and Actual Tasks on Multidisciplinary Sciences, 8-10 June, 2011, Lozanec, Bulgaria : third conference. Rousse : Bulgarian National Multidisciplinary Scientific Network of the Professional Society for Research Work. 2011, Vol. 3, p. 83-87.
18. Chanson, H. Turbulent air-water flows in hydraulic structures: dynamic similarity and scale effects. Environ. Fluid Mech. 9, 2009, p. 125-142.

19. Chanson, H. Bubbly flow structure in hydraulic jump. Eur. J. Mech. B/Fluids 26 (3), 2007, p. 367–384.
20. Pump, C.N. Air entrainment relationship with water discharge of vortex drop structures. M.Sc. thesis, The University of Iowa, 2011, p. 54.
21. Johansson, M.; Leifer, I.; Vamling, L.; Olausson L. Falling film hydrodynamics of black liquor under evaporative conditions. International Journal of Heat and Mass Transfer 52, 2009, p. 2769–2778.
22. Liang, J-H.; McWilliams, J. C.; Sullivan, P. P.; Baschek, B. Modeling bubbles and dissolved gases in the ocean. Journal of the Geografical Research 116, 2011, p. 1-17.
23. Vaideliene, A.; Mihailov, N. Dam influence on the river self - purification // Environmental Engineering : selected papers of the 7th international conference, May 22-23, 2008, Vilnius, Lithuania, Vol. 2 / Lthuanian Academy of Sciences, Federation of European Heating and Air-Conditioning Associations, Internal Federation of Surveyors, Baltic Road Association, ... [et al.]. Vilnius : Technika, 2008, p. 748-757.
24. Vaideliene, A.; Vaidelys, V. Mathematical simulation of aeration and diffusion processes in the air-water interface // Environmental Engineering : selected papers of the 8th international conference, May 19-20, 2011, Vilnius, Lithuania : Vol. 1, Environmental Protection / Edited by D. Cygas and K.D. Froehner. Vilnius : Technika. 2011, p. 401-407.
25. Vaideliene, A.; Vaidelys, V. Air bubbles and water droplets entrainment and removal in turbulent water flows. Mechanika 18(1), 2012, p. 56-62.
26. Chanson, H. Hydraulic jumps: turbulence and air bubble entrainment. La Houille Blanche 3, 2011, p. 5-16.
27. Vaideliene, A.; Tervydis, P. Measurement of air bubbles concentration in the water by means of digital image processing. Electronics and Electrical Engineering. Vol. 19(4), 2013, p. 77-80.
28. Vaideliene, A.; Galdikas A.; Tervydis, P. Modeling of Kinetics of Air Entrainment in Water Produced by Vertically Falling Water Flow. Materials science 20(3), 2013, p. 357-362.
29. Chanson, H. Convective transport of air bubbles in strong hydraulic jumps. International Journal of Multiphase Flow, 36 2010, p. 798-814.
30. Deswall, S. Modeling Oxygen-transfer by Multiple Plunging Jets using Support Vector Machines and Gaussian Process Regression Techniques. World Academy of Science, Engineering and Technology 73, 2011, p. 28-33.
31. Chanson, H.; Aoki, S.; Hoque, A. Physical modelling and similiyude of air bubble entrainment at vertical circular plunging jets. Chemical Engineering Science 59, 2004, p. 747-758.